



Contents lists available at ScienceDirect

## Surface &amp; Coatings Technology

journal homepage: [www.elsevier.com/locate/surfcoat](http://www.elsevier.com/locate/surfcoat)

# Orthorhombic Ta<sub>3-x</sub>N<sub>5-y</sub>O<sub>y</sub> thin films grown by unbalanced magnetron sputtering: The role of oxygen on structure, composition, and optical properties

Jui-Che Chang<sup>a</sup>, Fredrik Eriksson<sup>a</sup>, Mauricio A. Sortica<sup>b</sup>, Grzegorz Greczynski<sup>a</sup>, Babak Bakht<sup>a</sup>, Zhangjun Hu<sup>c</sup>, Daniel Primetzhofer<sup>b,d</sup>, Lars Hultman<sup>a</sup>, Jens Birch<sup>a</sup>, Ching-Lien Hsiao<sup>a,\*</sup>

<sup>a</sup> Division of Thin Film Physics, Department of Physics, Chemistry and Biology (IFM), Linköping University, Linköping SE 58183, Sweden

<sup>b</sup> Tandem Laboratory, Uppsala University, Uppsala SE 75120, Sweden

<sup>c</sup> Division of Molecular Surface Physics and Nanoscience, Department of Physics, Chemistry and Biology (IFM), Linköping University, Linköping SE 58183, Sweden

<sup>d</sup> Division of Applied Nuclear Physics, Department of Physics and Astronomy, Uppsala University, Uppsala SE 75120, Sweden

## ARTICLE INFO

## Keywords:

Ta<sub>3</sub>N<sub>5</sub>

Magnetron sputtering

XRD

XPS

ERDA

Optical absorption spectroscopy

## ABSTRACT

Direct growth of orthorhombic Ta<sub>3</sub>N<sub>5</sub>-type Ta-O-N compound thin films, specifically Ta<sub>3-x</sub>N<sub>5-y</sub>O<sub>y</sub>, on Si and sapphire substrates with various atomic fractions is realized by unbalanced magnetron sputtering. Low-degree fiber-textural Ta<sub>3-x</sub>N<sub>5-y</sub>O<sub>y</sub> films were grown through reactive sputtering of Ta in a gas mixture of N<sub>2</sub>, Ar, and O<sub>2</sub> with keeping a partial pressure ratio of 3:2:0.1 in a total working pressure range of 5–30 mTorr. With increasing total pressure from 5 to 30 mTorr, the atomic fraction of O in the as-grown Ta<sub>3-x</sub>N<sub>5-y</sub>O<sub>y</sub> films was found to increase from 0.02 to 0.15 while that of N and Ta decrease from 0.66 to 0.54 and 0.33 to 0.31, respectively, leading to a decrease in *b* lattice constant up to around 1.3%. Metallic Ta<sub>N</sub> phases were formed without oxygen. For a working pressure of 40 mTorr, an amorphous, O-rich Ta-N-O compound film with a high O fraction of ~0.48, was formed, mixed with non-stoichiometric TaON and Ta<sub>2</sub>O<sub>5</sub>. By analyzing the plasma discharge, the increasing O incorporation is associated with oxide formation on top of the Ta target due to a higher reactivity of Ta with O than with N. The increase of O incorporation in the films also leads to an optical bandgap widening from ~2.22 to ~2.96 eV, which is in agreement with the compositional and structural changes from a crystalline Ta<sub>3-x</sub>N<sub>5-y</sub>O<sub>y</sub> to an amorphous O-rich Ta-O-N compound.

## 1. Introduction

Photoelectrolyzing water into hydrogen and oxygen by renewable electricity is a possible method to produce clean hydrogen. Most conventional setups consist of a semiconducting TiO<sub>2</sub> electrode which often shows low efficiency for water splitting [1]. Other oxide semiconductors, such as Fe<sub>2</sub>O<sub>3</sub>, Cu<sub>2</sub>O [2], and WO<sub>3</sub> [3] have been studied as photoanodes because of their stability. However, these materials suffer from various limitations such as large bandgaps and improper band edge positions for water splitting. Semiconductor orthorhombic tritantalum pentanitride (Ta<sub>3</sub>N<sub>5</sub>) is one of the most promising materials for the photoelectrolysis of water owing to a proper energy gap of 2.0 ± 0.2 eV [4–8] and suitable band positions with respect to the redox potential of water [9,10]. Related, monoclinic and bixbyite tantalum oxynitrides (TaO<sub>x</sub>N<sub>y</sub>) and with a bandgap range of 2.4–2.8 eV [5–7,11] and ~2 eV

[12], respectively, were also demonstrated to have a good response for water splitting although its valence band energy is lower than Ta<sub>3</sub>N<sub>5</sub>. Therefore, the Ta-O-N compounds are promising materials with tunable bandgap and band positions to fit a desired value for the water splitting.

Conventionally, Ta<sub>3</sub>N<sub>5</sub> is produced through a two-step process of oxidation and nitridation of a Ta metal foil. However, the amount of incorporated oxygen in the Ta<sub>3</sub>N<sub>5</sub> samples and film's thickness are hardly to be controlled [7,13], and the use of ammonia as the nitridation gas is harmful to the environment. It should be noted that regardless of how much oxygen that is incorporated into the films, the chemical formula Ta<sub>3</sub>N<sub>5</sub> is used as a generic name. Direct, single-step, growth of Ta<sub>3</sub>N<sub>5</sub> onto various types of substrates using atomic layer deposition [14,15] and reactive magnetron sputtering are reported [8,16–18], which demonstrates several advantages, such as simplification of the deposition process, growth on nanostructured substrates, and hetero-

\* Corresponding author.

E-mail address: [Ching-lien.hsiao@liu.se](mailto:Ching-lien.hsiao@liu.se) (C.-L. Hsiao).

<https://doi.org/10.1016/j.surfcoat.2020.126665>

Received 5 October 2020; Received in revised form 14 November 2020; Accepted 18 November 2020

Available online 19 November 2020

0257-8972/© 2020 The Authors. Published by Elsevier B.V. This is an open access article under the CC BY license (<http://creativecommons.org/licenses/by/4.0/>).

growth of multilayers with other potential materials. Moreover, magnetron sputtering has the potential to scale up for industrial production and enables use of the environmentally-friendly reactive gases argon (Ar), nitrogen ( $N_2$ ) and oxygen ( $O_2$ ) to produce high-quality semiconductors [18–21].

To date, studies on the direct growth of  $Ta_3N_5$  are limited in number due to the nature of metastable structures in the complex system of Ta–N binary compounds [22,23]. Direct growth of  $TaN_x$  often results in the formation of stable metallic cubic phases, mostly  $\delta$ - $TaN_x$  and  $\epsilon$ - $TaN_x$  [22]. Despite that the concentration ratio of N to Ta in sputtered  $TaN_x$  films can be higher than 1.67, the film is preferable to be grown in cubic TaN phase with excess N rather than in the orthorhombic  $Ta_3N_5$  phase ( $x = 1.67$ ). Calculations predict that a small number of oxygen atoms incorporated in the film can stabilize an orthorhombic  $Ta_3N_5$  structure through the electronegativity enhancement induced by the oxygen [24]. M. Rudolph et al. successfully produced polycrystalline  $Ta_3N_5$  films by direct current (DC) magnetron sputtering using a balanced magnetic configuration, by introducing a small amount of oxygen in the range of 2–2.5% into the reactive gas [8]. The crystallinity of the sputtered  $Ta_3N_5$  films can be further improved by increasing ion flux to the growing film by using an electromagnetic coil to attract ions to the substrate [16]. Although the direct growth of sputtering  $Ta_3N_5$ -type films is progressing, the study of incorporated oxygen on the control of crystalline structure, chemical composition and bonding, and optical properties of as-grown Ta–O–N films as well as the effect of oxygen in reactive sputtering process is rarely reported [8]. Be specific, more studies on the process control and incorporated oxygen on the materials properties are required for developing the growth high-quality  $Ta_3N_5$  films, such as single crystalline structure and stoichiometry, aiming for application of high efficiency water splitting.

In this work, ultrahigh vacuum (UHV), unbalanced, DC magnetron sputtering (DCMS) [25] was used to deposit  $Ta_{3-x}N_{5-y}O_y$  compound films with varying total working pressure to introduce a small amount of oxygen. To illustrate the difference to pure  $Ta_3N_5$  crystals, a chemical formula  $Ta_{3-x}N_{5-y}O_y$  is used to present the orthorhombic  $Ta_3N_5$ -type  $TaO_xN_y$  compounds. The UHV condition of the system enables to eliminate possible contribution of oxygen originating from the residual background gas. The use of unbalanced magnetic configuration can guide the plasma towards the substrate resulting in enhancement of kinetic energy with ion assistant, which simplifies the process [26,27]. To study the effects of oxygen on structure, composition, and optical properties of the as-grown films, several characterization techniques were used. The crystalline structure and chemical composition of the as-grown films were characterized by X-ray diffraction (XRD), X-ray photoelectron spectroscopy (XPS), and elastic recoil detection analysis (ERDA). Optical emission spectroscopy (OES) was used to analyze the plasma discharge properties during the reactive magnetron sputtering growth. The energy band gap of the films was determined by optical absorption spectroscopy (OAS). The role of oxygen in the formed  $Ta_3N_5$  structure, chemical composition and bonding, optical properties, and sputtering process are discussed.

## 2. Experiments

### 2.1. Materials growth

The films were deposited on single crystal n-type Si (111) and sapphire  $Al_2O_3$  (0001) substrates using UHV DCMS [28]. Both substrates were deposited at the same time. An unbalanced type-II magnetron configuration was used for guiding the plasma towards the substrate. Before deposition, the substrate was cleaned in ultrasonic baths with acetone and isopropanol ultrasonic baths for 5 min each and dried by blowing nitrogen. The substrate was then loaded in a load-lock chamber and transferred to the deposition chamber. A continuous substrate rotation of 30 rpm was applied to ensure a homogeneous film during deposition. First, a thin amorphous  $TaN_xO_y$  seed layer was deposited at

room temperature and annealed at 1000 °C to minimize the effect of any substrate surface structure. For the growth of oxygen-free samples, reactive sputter deposition of a 75 mm-diameter Ta target (99.99%) using a gas mixture of  $N_2$  and Ar with the partial pressures of 3 and 2 mTorr, respectively, was employed at 800 °C. The magnetron power and deposition time were set to 150 W and 20 min, respectively. For samples grown with oxygen, a partial pressure of 0.1 mTorr oxygen was introduced to the gas mixture with a partial pressure of 3 mTorr  $N_2$  and 2 mTorr Ar, corresponding to ~2% of the total pressure. Keeping the same partial pressure ratio ( $N_2:Ar:O_2 = 3:2:0.1$ ), six samples were deposited at total working pressures of around 5, 10, 15, 20, 30, and 40 mTorr by throttling the main chamber turbopump. All oxygen-containing samples were deposited at 800 °C, for 20 min and the magnetron power was set at 300 W.

### 2.2. Sample characterizations

Structural property was obtained from XRD  $\theta/2\theta$  measurement, performed using a Philips Bragg-Brentano powder diffractometer using Cu-K $\alpha$  radiation with a wavelength of 0.15406 nm. A scan range of 15° to 60° was used with a step size of 0.03° and a collection time of 2 s/step.

XPS analysis of surface chemistry was carried out on a Kratos Axis Ultra DLD instrument employing monochromatic Al K $\alpha$  radiation ( $h\nu = 1486.6$  eV). The spectra are referenced to the Fermi edge cut-off [29,30] to avoid uncertainties associated with using the C 1s peak of adventitious carbon for that purpose [31]. The analyzer pass energy was set to 20 eV which resulted in a full width at half maximum of 0.55 eV for the Ag 3d $_{5/2}$  peak. Quantification of the elements in the samples was performed using the Casa XPS software (version 2.3.16), based upon peak areas from narrow energy range scans and elemental sensitivity factors supplied by Kratos Analytical Ltd.

The chemical composition of the films, with a particular focus on light species such as C, N, and O was analyzed by heavy ion time-of-flight ERDA. A primary beam of iodine ions with an energy of 36 MeV was used in the experiments. The measurements were carried out at a recoil detection angle ( $\varphi$ ) equal to 45° with respect to the primary beam and a target angle ( $\beta$ ) equal to 22.5° with respect to the sample surface, using a 0.425 m effective length of the time-of-flight distance. Since the accuracy of the results decreases with increasing depth due to multiple scattering effects in ERDA, the analyzed data was averaged in the depth region 50–200  $\cdot 10^{15}$  atoms/cm $^2$  for  $\delta$ -TaN sample and 50–500  $\cdot 10^{15}$  atoms /cm $^2$  for Ta–O–N compounds samples. It should be noted that when comparing different samples, concentration ratios (atomic fractions) are less affected by systematic uncertainties than absolute concentrations. This fact allows relying even on weak trends in concentrations for different deposition conditions. A detailed discussion of possible systematic uncertainties can be found elsewhere [32].

OES was performed to characterize the plasma during sputtering using a Ifu Diagnostic Systems GmbH AOS 4–1  $\mu$ chro 02. Before the measurement, the instrument was calibrated to the spectrum of neon. The emitted photons from the plasma were collected by an optical fiber to OES and sent to the spectrometer via a viewport in the chamber. Because of photon absorption by the viewport at wavelengths shorter than 400 nm, the scanning range was set to 400–800 nm and a 1-nm step size was used. The collection time for each step was 0.01 s and the voltage to the photo multiplier tube was set to 1000 V.

Ultraviolet-visible spectrophotometer (Shimadzu, UV-2450) was used for OAS measuring the band gaps of the films grown on sapphire substrates. It should be noted that Si has a smaller band gap (1.1 eV) than  $Ta_{3-x}N_{5-y}O_y$  ( $> 2.1$  eV) and can absorb photon energy larger than band gap, which is not the proper substrate used for this OAS measurement. Herein, the sapphire was used as the substrates and the absorption spectrum of sapphire was measured as background. The spectra were collected in the range of 250–900 nm. The band gaps for the samples were calculated utilizing the Tauc method.

### 3. Results and discussion

#### 3.1. Structure and chemical composition of as-grown films

##### 3.1.1. Crystalline structure

The crystalline structures of as-grown films was characterized by  $\theta/2\theta$ -scan XRD and are shown in Fig. 1. From films deposited without introducing oxygen in the reactive gas, the diffractogram showed one high intensity peak located at  $2\theta = 35.89^\circ$ , and one low intensity peak at  $2\theta = 41.67^\circ$ , corresponding to the 111 and 200 diffraction peaks of cubic  $\delta$ -TaN according to the inorganic crystal structure database (ICSD) pattern no.07-6456, in addition to the 111 and 222 Si substrate peaks at  $2\theta = 28.56$  and  $58.86^\circ$ , see Fig. 1(a). Below the measurement, the diffraction histogram for cubic  $\delta$ -TaN is shown, and the diffraction pattern indicates that the sample was grown preferentially along 111 orientation. When introducing  $\sim 2\%$  of  $O_2$  into the gas mixture of Ar and  $N_2$  during growth, the XRD measurement for the sample grown at 5 mTorr total pressure shows very different patterns to  $\delta$ -TaN. Multiple diffraction peaks located at  $2\theta = 17.35, 31.45, 35.02, 36.04, 39.33$ , and  $53.82^\circ$  were measured, as shown in Fig. 1(b), revealing a polycrystalline structure. These peaks correspond to 020/002, 023, 040/004, 113, 042/024, and 060/006 planes of orthorhombic  $Ta_3N_5$ , respectively, plotted in the bottom of the figure according to ICSD pattern no.06-6533. The orthorhombic  $Ta_3N_5$  structure belongs to the space group of  $CmCm$  with lattice constants of  $a = 3.89 \text{ \AA}$ ,  $b = 10.21 \text{ \AA}$ , and  $c = 10.26 \text{ \AA}$ . Since the difference between  $b$  and  $c$  lattice constants is only  $\sim 0.05 \text{ \AA}$ , the family of XRD peaks  $\{0k0\}$  and  $\{00l\}$ , where  $k = l$ , become difficult to distinguish and are presented in the form of  $\{0l0\}/\{00l\}$  in this study. The above results show that the  $O_2$  is an important gas to trigger the formation of orthorhombic  $Ta_3N_5$  phase.

The effect of total working pressure on the crystalline structure was studied by changing the total pressure from 5 to 40 mTorr while keeping the same partial pressure ratio ( $N_2:Ar:O_2 = 3:2:0.1$ ). Fig. 1(c) shows that the  $Ta_3N_5$  phase remains, and a transition from polycrystalline to a fiber-texture-like structure with prefer orientation dominated by  $\{0l0\}/\{00l\}$  occurs with increasing pressure from 5 to 30 mTorr. At a further increase in working pressure up to 40 mTorr, the film becomes amorphous. In addition, the peaks of  $\{0l0\}/\{00l\}$  of  $Ta_3N_5$  films slightly shift to higher diffraction angles when the total working pressure increases from 5 to 30 mTorr indicating a decreasing interplanar spacing. Due to the orthorhombic structure, the  $a$ ,  $b$ , and  $c$  lattice constants can easily be obtained from  $d_{hkl}$ -spacing of  $(h00)$ ,  $(0k0)$ , and  $(00l)$  with formulas of  $h \cdot d_{h00}$ ,  $k \cdot d_{0k0}$ , and  $l \cdot d_{00l}$ , respectively. The  $b$ - or  $c$ -lattice constant of the  $Ta_3N_5$  crystal versus working pressure is plotted in Fig. 1(d), which shows a clear decrease in lattice constant with increasing pressure, and the largest lattice constant difference between 5- and 30-mTorr samples is  $0.13 \text{ \AA}$  ( $\sim 1.3\%$  of  $b$  or  $c$  lattice constant).

##### 3.1.2. Chemical bonding

The films were further characterized by XPS to study the bonding structure. Fig. 2(a) and (b) show sets of XPS Ta 4f and N 1s core-level spectra, respectively, from TaN, 5, 30, and 40 mTorr samples. To avoid destructive effects of the  $Ar^+$  ion etch, the results shown in Fig. 2 (a) and (b) were obtained directly from as-grown films without surface sputtering.

Fig. 2(a) shows that all Ta 4f spectra consist of two main peaks, which are attributed to  $4f_{7/2}$  and  $4f_{5/2}$  spin-split components. For the sample grown without oxygen,  $N_2:Ar = 3:2$ , the two Ta 4f peaks are located at 23.6 and 25.5 eV, see the bottom most spectra in Fig. 2(a), indicating formation of  $\delta$ -phase TaN [33–36]. This is further confirmed

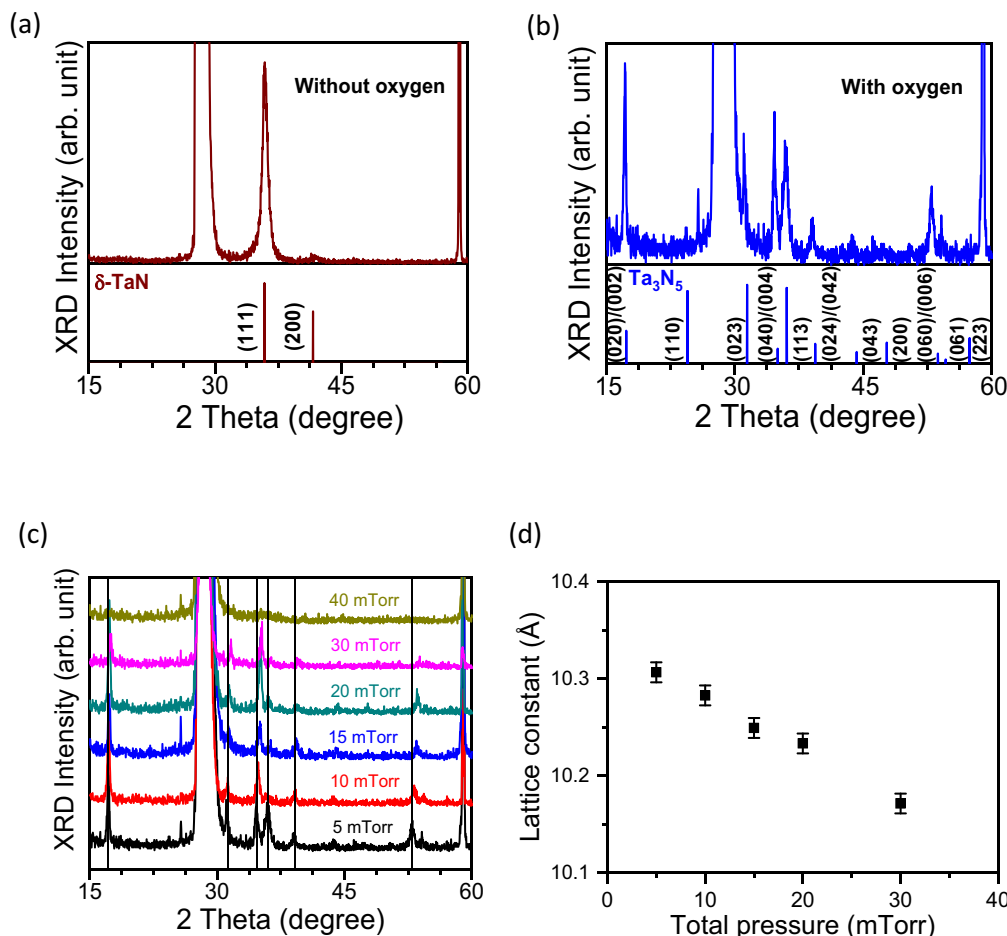


**Fig. 1.** X-ray diffraction (XRD) results of as-grown films. (a) Sample grown without oxygen assistance, (b) Sample grown with oxygen assistance ( $\sim 2\%$  in a total working pressure of 5 mTorr). The bottom patterns of (a) and (b) are plotted according to ICSD patterns no. 07-6456 and 06-6533, respectively. (c) Samples grown in a total working pressure range from 5 to 40 mTorr, while keeping the same partial pressure ratio ( $\sim 2\%$  oxygen). The black guiding lines are diffraction peaks of 5 mTorr sample. (d) The corresponding  $b$  or  $c$  lattice constant versus the total working pressure of the samples grown from 5 to 30 mTorr. The lattice constant is calculated from the (020)/(002). The error-bar is  $0.01 \text{ \AA}$ .

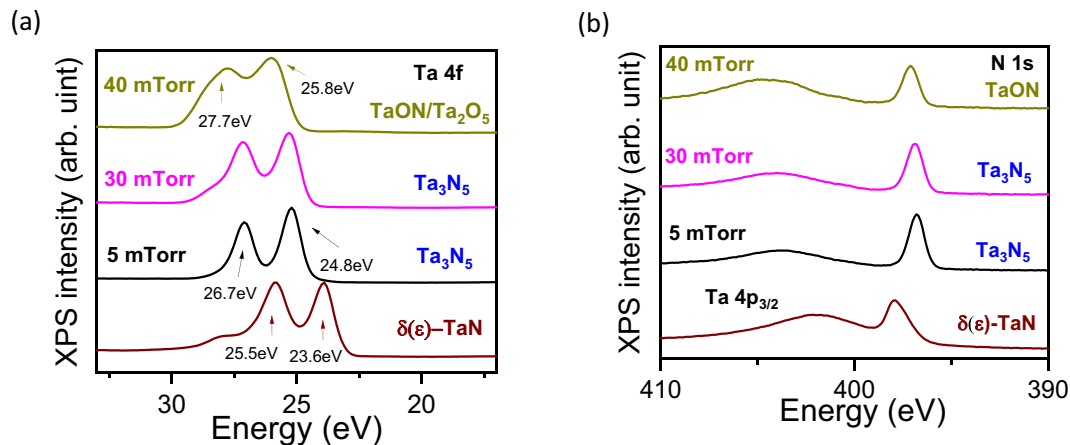


**Fig. 2.** (a) Ta 4f and (b) N 1s and Ta 2p core level X-ray photoelectron spectroscopy (XPS) spectra of TaN sample (without oxygen), 5, 30, and 40 mTorr samples (~2% oxygen in gas mixture for all working pressures).

by the relatively high binding energy of the corresponding N 1s peak, 397.8 eV, see the bottom most spectrum in Fig. 2(b), as well as XRD results, see Fig. 1(a). A small shoulder visible on the high binding energy side of the Ta  $4f_{5/2}$  peak at around 27.8 eV is assigned to the residual Ta—O [29]. For samples grown at 5 mTorr gas mixture with ~2% of oxygen,  $N_2:Ar:O_2 = 3:2:0.1$ , the Ta 4f peaks shift towards higher binding energies with  $4f_{7/2}$  and  $4f_{5/2}$  peaks at 26.7 and 24.8 eV, respectively, while the corresponding N 1s peak moves in the opposite direction to 396.7 eV, indicating  $Ta_3N_5$  formation [6,34,37–40]. Observed binding energy (BE) shifts reveal an increased charge transfer between Ta and N

atoms (with respect to the  $\delta$ -TaN), which likely results from the higher N coordination number and shorter Ta—N bond length [41]. Sample deposited at 30 mTorr shows essentially the same result. These spectra confirm the formation of  $Ta_3N_5$ -type Ta-N-O compound. However, in the case of the 40-mTorr sample, the Ta 4f spectrum shows evidence for the Ta-oxide formation, as the peaks move to higher BE and become broader, which is characteristic of phase mixture. Spectra deconvolution suggests the presence of monolithic TaON phase (Ta  $4f_{7/2}$ : 25.8 eV, Ta  $4f_{5/2}$ : 27.7 eV [6,36]) and  $Ta_2O_5$  phase (Ta  $4f_{7/2}$ : 26.6 eV, Ta  $4f_{5/2}$ : 28.5 eV [42]). Evidence for residual amount of  $Ta_2O_5$  is also evident in the 30

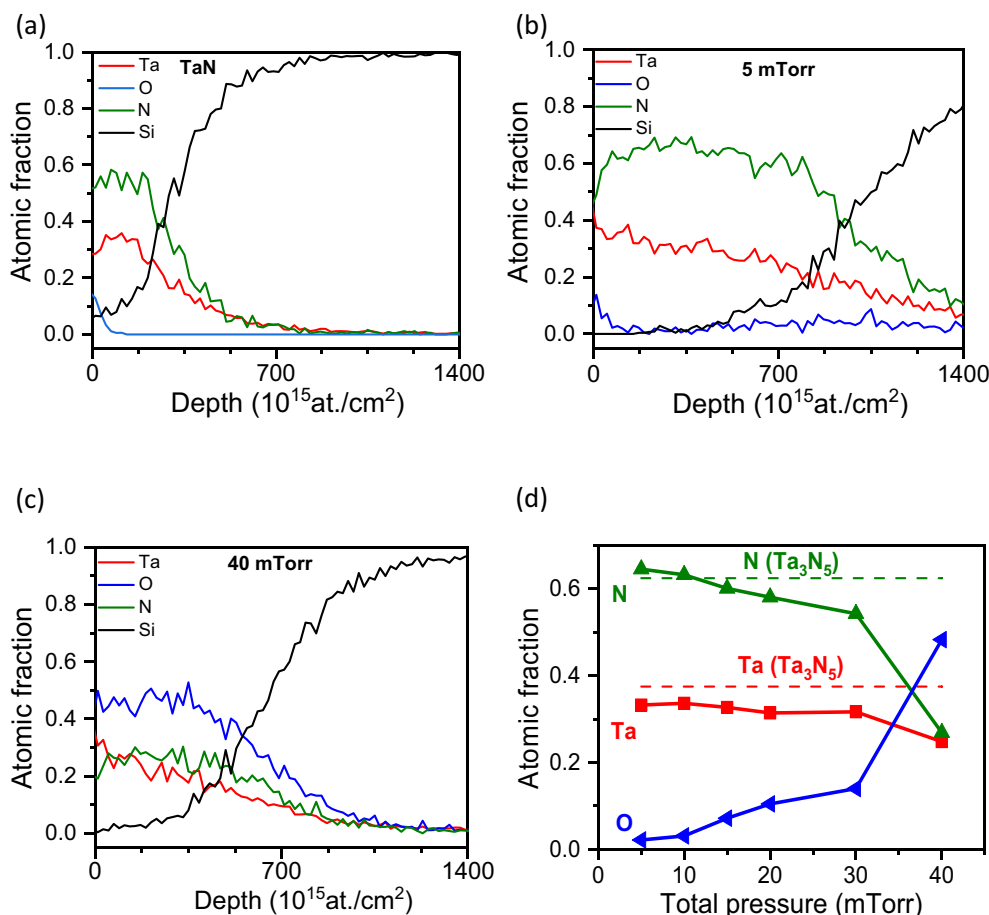


**Fig. 3.** Analysis of chemical composition determined by elastic recoil detection analysis (ERDA). Elemental depth profiles obtained by (a)  $\delta$ -TaN sample, (b) 5-mTorr, and (c) 40-mTorr samples. (d) Total working pressure versus atomic fraction, Ta, N, and O, of samples deposited at 5, 10, 15, 20, 30, and 40 mTorr (keeping ~2% of  $O_2$  in gas mixture for all working pressures). The value is the average between  $50 \cdot 10^{15}$  atoms/cm<sup>2</sup> and  $500 \cdot 10^{15}$  atoms/cm<sup>2</sup>. Note: the Ta, N, and O atomic fractions are summed up to 1. The dash lines label the fraction of pure  $Ta_3N_5$ .



mTorr sample.

### 3.1.3. Chemical composition

To study the stoichiometry of as-grown samples, ERDA is used to quantify the chemical composition. Fig. 3(a), (b), and (c) are three representative depth profiles measured from the TaN, 5 and 40 mTorr samples to show oxygen-free, low- and high-incorporation of oxygen films, respectively. Apart from information on the atomic fraction of elements in the films, the depth profiles allow also to obtain thickness information if density of the films is known. From Si profiles, a trend of thickness variation gives a result of sample 5 mTorr > 40 mTorr >  $\delta$ -TaN, which also refers to the same correspondence in deposition rate at a fixed deposition time. The result of thickness trend is in agreement with the thickness measured from scanning electron microscopy (not shown here), which the thickness of 5 mTorr, 40 mTorr and  $\delta$ -TaN is around 124, 101, and 56 nm, respectively.

Fig. 3(a) shows an ERDA depth profile of the  $\delta$ -TaN film grown in a gas mixture with only Ar and N<sub>2</sub>. The Ta and N profiles show the same trend oppositely to Si throughout the entire regime. Although the signal of Si is seen from the beginning of the depth profile due to the small thickness of the film makes energy loss straggling of more heavy species problematic and smears out the energy profile, the N/Ta ratio is not expected to be significantly affected, as long as the profiles of these two are proportional to each other. The atomic fractions of Ta and N in the film are 0.324 and 0.546, respectively, which yields a N/Ta ratio around 1.67, indicating an over-stoichiometry from excess N. The high N/Ta ratio is in fact equivalent to the stoichiometry of Ta<sub>3</sub>N<sub>5</sub> phase. The signal of O is only seen clearly on the surface, confirming the oxidation of top layer when the sample was exposed to air. The amount of O inside the film is close to the detection limit (<1%). Fig. 3(b) shows the ERDA depth profile of 5 mTorr Ta<sub>3</sub>N<sub>5</sub> sample. The atomic fractions of Ta, N, and O in the film are 0.333 and 0.656, and 0.022, respectively. The non-metal elements, N + O, to Ta ratio reveals an over stoichiometry of 2.03 instead of 1.67. This over-stoichiometry is mainly contributed from excess N because the atomic fraction of O in the film is as low as around 0.022, neglecting the surface oxide. The O incorporation in the film increases dramatically when deposition made in total pressure of 40 mTorr, as can be seen in Fig. 3(c). The atomic fraction of O becomes 0.483 while N and Ta drop to 0.269 and 0.248, respectively.

The atomic fraction of Ta, N and O elements plotted as a function of total working pressure (keeping the same partial pressure ratio of gas mixture) is shown in Fig. 3(d). When the pressure is increased from 5 to 30 mTorr, the atomic fraction of incorporated O increases monotonically with pressure while the trend of N behaves oppositely. The corresponding fraction of O in total non-metal elements, O/(O + N), increases from 0.03 to 0.21. Nevertheless, the atomic fraction for the non-metal elements in the films is almost constant, with only a slight increase from 0.67 to 0.69, indicating that the incorporated O atoms are mostly replacing N atoms in the films. Meanwhile, the atomic fraction of Ta decreases only slightly with pressure. The ratio of total non-metal to metal constituents hence increases from 2.03 to 2.20 with increasing

pressure from 5 to 30 mTorr, revealing always over stoichiometry and an excess non-metal constituents in the orthorhombic Ta<sub>3-x</sub>N<sub>5-y</sub>O<sub>y</sub> films. The stoichiometric condition of the film grown at 40 mTorr pressure reveals an abrupt change in comparison to the films grown at lower pressure regime. The atomic fraction of O becomes almost twice as high as N, and (O + N)/Ta ratio is over 3. The result indicates a high possibility of phase transition from Ta<sub>3</sub>N<sub>5</sub> type structure to a mixing phase with TaON and Ta<sub>2</sub>O<sub>5</sub> as the results, as obtained from XPS measurement, implying that O takes main role in reaction with Ta to form a new phase. Hence, the film dominated by Ta-oxide compounds is referred to as amorphous O-rich TaN<sub>x</sub>O<sub>y</sub>.

### 3.1.4. Discussions on structural properties of as-grown films

The results of XRD, XPS, and ERDA, summarized in Table 1, show that the crystalline structure and chemical composition of Ta-N-O compound films are highly sensitive to the growth conditions. Oxygen is found to be a decisive role to alter forming the crystalline structures of the sputtered films from  $\delta$ -TaN to orthorhombic Ta<sub>3</sub>N<sub>5</sub>-type Ta<sub>3-x</sub>N<sub>5-y</sub>O<sub>y</sub> and to amorphous O-rich TaN<sub>x</sub>O<sub>y</sub> compounds when the process gas was added with a small of oxygen and increased with working pressure.

By adding ~2% of oxygen in the process gas, the crystalline Ta<sub>3</sub>N<sub>5</sub>-type structure was formed and stabilized. We also made attempts to grow Ta<sub>3</sub>N<sub>5</sub> without oxygen assistance by varying growth conditions, such as temperature, the partial pressure ratio of N to Ar, magnetron power, and the use of substrate. However, only metallic TaN compounds, including  $\delta$ -TaN,  $\epsilon$ -TaN, and other TaN<sub>x</sub> (x < 1) films, were formed in our depositions (not shown here), which is in agreement with a previous report [22] for the difficulty in growing Ta<sub>3</sub>N<sub>5</sub> films. The effect of oxygen, which increases the stability of a compound with high-oxidation-state transition metal atoms by replacing its bonding partner with an atom having a higher electronegativity, called inductive effect [24], triggers the formation of crystalline Ta<sub>3</sub>N<sub>5</sub>-type structure. In addition, the oxygen is seeming incorporated into the growth, but not only acts as a role of catalyst, as seen in the results of XPS and ERDA.

The stability of metastable Ta<sub>3</sub>N<sub>5</sub> structure was studied by modelling structure from a 96-atom orthorhombic Ta<sub>3</sub>N<sub>5</sub> supercell using density-functional theory (DFT), reported by Harb et al. [7]. Their calculation showed much enhancement in structural stability by partial replacement of nitrogen with oxygen in the model, which five neutral N atoms at specific sites having two N4, two N5 and one N3 sites [43] were replaced by five O atoms, on b planes. Such a replacement results in the change of b lattice constant more than a and c lattice constant and generation of one Ta vacancy. The chemical formula of the compound was hence referred to as Ta<sub>3-x</sub>N<sub>(5-5x)</sub>O<sub>5x</sub>. The incorporated oxygen atoms in the crystal were mainly contributed to the substitutional and unavoidable. In addition, the formation energy of intrinsic defects using spin-polarized DFT calculation reported by Jing et al. also shows that the substitution of O for N is the most stable among all of defects in Ta<sub>3</sub>N<sub>5</sub> [44]. The results in their modelling are consistent with our ERDA result that the trend of O and N varied oppositely with working pressure shown in Fig. 3(d). Assuming all incorporated O atoms substitute N sites, the

**Table 1**  
Summarized results of XRD, XPS, and ERDA.

Sample	XRD		XPS	ERDA			
	Crystalline structure	<sup>a</sup> Lattice const. (Å)		Atomic fraction			(O + N)/Ta
			Bonding type	Ta	N	O	
TaN	$\delta$ -TaN	4.33	TaN	0.323	0.546	–	1.67
5 mTorr	Ta <sub>3</sub> N <sub>5</sub>	10.30	Ta <sub>3</sub> N <sub>5</sub>	0.333	0.656	0.022	2.04
10 mTorr	Ta <sub>3</sub> N <sub>5</sub>	10.28	Ta <sub>3</sub> N <sub>5</sub>	0.336	0.633	0.031	1.98
15 mTorr	Ta <sub>3</sub> N <sub>5</sub>	10.25	Ta <sub>3</sub> N <sub>5</sub>	0.327	0.601	0.072	2.08
20 mTorr	Ta <sub>3</sub> N <sub>5</sub>	10.23	Ta <sub>3</sub> N <sub>5</sub>	0.314	0.581	0.105	2.16
30 mTorr	Ta <sub>3</sub> N <sub>5</sub>	10.17	Ta <sub>3</sub> N <sub>5</sub> + TaON	0.317	0.543	0.148	2.20
40 mTorr	Amorphous	–	TaON + Ta <sub>2</sub> O <sub>5</sub>	0.248	0.269	0.483	3.03

<sup>a</sup> Sample-TaN: a lattice constant of  $\delta$ -TaN; Samples with Ta<sub>3</sub>N<sub>5</sub>-type structure: b or c lattice constant.

ratio of non-metal to metal,  $(N + O)/Ta$ , of stoichiometric  $Ta_{3-x}N_{5-y}O_y$  films should be kept at 1.67. However, an over stoichiometry of excess non-metal elements of the as-grown films was always obtained from ERDA, see Table 1. By calculating the elemental ratio according to Harb's assumption of chemical formula  $Ta_{3-x}N_{(5-5x)}O_{5x}$  using O atomic fraction obtained from ERDA as the base, we find that over stoichiometry of these films is mainly associated with excess N and deficiency of Ta atoms, which may result in the generation of N interstitials and Ta vacancies, in the pressure region of 5–30 mTorr. Other defects, such as O and Ta interstitials and N vacancies, with higher formation energy cannot be completely excluded since they may be generated by energetic reactive species in magnetron sputtering process. Among them, O interstitials have high possibility to be increased with pressure as the non-metal atomic fraction does not change too much. However, contribution of other defects in determining the non-metal to metal ratio is relatively low. The N becomes deficiency, and the over stoichiometry of non-metal elements is even higher in 40-mTorr sample,  $(N + O)/Ta = 3.03$ , if the structure is kept in orthorhombic  $Ta_3N_5$ -type phase. This transition indicates that the constitution of the film becomes oxide dominant rather than nitride, which matches the present XPS result that the film contains  $Ta_2O_5$  and  $TaON$  compounds. In addition, previous study shows that the formation of crystalline O-rich  $TaO_xN_y$  film requires annealing temperature higher than 900 °C [11]. Hence, the O-rich  $TaO_xN_y$  film grown at 800 °C is thought too low to form crystalline.

The confirmation of forming  $Ta_{3-x}N_{5-y}O_y$  compound alloys with varied atomic fraction further explains the decrement of  $b$  or  $c$  lattice constant of the films grown with increasing working pressure from 5 to 30 mTorr, see Fig. 1(d) and Table 1. For 5-mTorr sample, the obtained lattice constant is 10.30 Å, which is larger than the  $b$  lattice constant of  $Ta_3N_5$  crystal, 10.21 Å, shown in ICSD database. (It should be noted that the O content was not specified in the database.) As the O atomic fraction is as low 0.022, this deviation in lattice constant is mainly associated with the formation of excess interstitial N atoms, which contributes isotropic tensile strain component to the film, as seen in other nitride films with over stoichiometry of N [45]. With increasing atomic fraction of O, the  $b$  or  $c$  lattice constant of  $Ta_{3-x}N_{5-y}O_y$  compounds becomes smaller. The shortest lattice constant obtained from the 30-mTorr sample is 10.17 Å, which has an around 1.3% decrement (0.13 Å) compared to 5-mTorr sample. Similar result was also obtained from conventional two-step growth  $Ta_{3-x}N_{5-y}O_y$  compounds, produced by nitriding (ammonia gas) the powder formed by stirring  $TaCl_5$  with ethanol under flowing ammonia gas and then pouring into dilute aqueous ammonia. Henderson et al. determined the change of lattice constant with O atomic fraction in the  $Ta_{3-x}N_{5-y}O_y$  compounds using powder neutron diffraction (PND) [43]. They found that both  $b$  and  $c$  lattice constants decrease from 10.23 to 10.18 Å and 10.28 to 10.26 Å, respectively, with increasing O atomic fraction from 0.03 to 0.07, while  $a$  lattice constant has almost no change. The change in  $b$  lattice constant is much more than  $a$  and  $c$  lattice constants with increasing O atomic fraction to around 0.07, which implies that the peaks of  $\{010\}/\{00l\}$  obtained in XRD of the  $Ta_{3-x}N_{5-y}O_y$  films are more have higher preference to be  $\{010\}$ . Furthermore, the lattice constant of  $Ta_{3-x}N_{5-y}O_y$  calculated by DFT method from Harb et al. also predicted the same trend that  $b$  and  $c$  lattice constants decrease monotonically with increasing O incorporation. A structure with higher atomic fraction of O  $\sim 0.16$  ( $Ta_{2.75}N_{3.75}O_{1.25}$ ) was predicted to have  $b$  lattice constant of 10.18 Å, which is 0.07 Å shorter than pure  $Ta_3N_5$ . The theoretical values obtained by the model, five O occupied N site surrounding with one Ta vacancy, is consistence with our experimental results. Therefore, the possible reasons of the decrement in lattice constant with increasing O incorporation are attributed to that 1) the small difference in the ionic radius that the  $O^{2-}$  is around 0.08 Å shorter than that of  $N^{3-}$  in  $Ta_{3-x}N_{5-y}O_y$  crystal [46], and 2) the Ta vacancy generated when O atoms replace N atoms at specific anion sites [7,43].

### 3.2. Reactive species

Because the partial pressure ratio of  $O_2$  in the gas mixture was fixed at  $\sim 2\%$  ( $N_2:Ar:O_2 = 3:2:0.1$ ), the result that increase of incorporated O in the films with total pressure is noteworthy. Therefore, the in-situ OES technique was used to characterize the plasma during the sputtering in a total working pressure range of 5–40 mTorr. Fig. 4(a) shows the emission spectra of the plasma generated by  $\sim 40$  mTorr in gas mixture of  $Ar + N_2$  (top) and  $Ar + N_2 + O_2$  (bottom). The spectra can be divided into three dominant regions: i) Three sharp-emission peaks from Ta located at 534, 539, and 581 nm [47]; ii) fingerprint envelop from molecular nitrogen emission in 620–690 nm; and iii) fingerprint envelop from atomic nitrogen emission in 710–780 nm. Since the emission from oxygen transitions overlaps (777.4 nm) [48], with nitrogen transitions, the difference in intensity of the fingerprint envelopes should be observed when the ratio of oxygen partial pressure changes. By comparing these two spectra, no obvious difference is seen in the region of nitrogen dominated emissions, indicating that the oxygen partial pressure ratio is still very low. However, the intensity of Ta transition peaks drops drastically in the gas mixture with oxygen, implying that the sputtering yield of Ta decreases.

Fig. 4(b) shows the dependence of intensity's difference of Ta transitions before and after O injection plotted as a function of total working pressure. Deviation of Ta transition's intensity becomes larger as increasing working pressure, indicating a higher reduction in Ta sputtering yield. The lower sputtering yield is expected to have a lower growth rate. From ERDA measurement, the lower growth rate is confirmed as the thickness of 40-mTorr sample is indeed less than 5-mTorr sample, see Fig. 3(b) and (c). The results shown above imply that O has higher reactivity to Ta in comparison to N, which is in line with the fact that metal has higher affinity to oxygen than nitrogen and a more negative enthalpy of formation of tantalum pentaoxide ( $-488.8$  kcal/mol) in comparison to tantalum nitride ( $-60.0$  kcal/mol) at 25 °C [49,50]. Although the partial pressure ratio of  $O_2$  in the process gas is kept as  $\sim 2\%$ , total amount of  $O_2$  still increases with increasing total working pressure. More oxides can be formed on the top of Ta target, which results in a higher degree of target poisoning. The sputtering yield of an oxide layer on Ta target is less than pure Ta target, but reactive species contain higher O, which leads to a higher amount of O incorporated into the deposited film. The OES result hence explains the peculiarity that the O atomic fraction in the films increases noteworthy from 0.022 to 0.486 with total pressure varying from 5 to 40 mTorr at a kept  $\sim 2\%$   $O_2$  in the processing gas mixture,  $N_2:Ar:O_2 = 3:2:0.1$ .

### 3.3. Optical properties

The effect of incorporated O in the films on the optical property of Ta-O-N samples was determined by OAS at room temperature. Tauc's method was used to determine band tails and the optical bandgaps from the optical absorption spectra of the samples. The plot is based on Tauc's equation  $(A\hbar\nu)^n = B(\hbar\nu - E_g)$  and  $n = 1/2$  is used for indirect bandgap materials [51], where  $A$  is the absorption coefficient,  $B$  is a constant,  $\nu$  is the angular frequency of incident radiation,  $h$  is Planck's constant, and  $E_g$  is the bandgap.  $E_g$  can be extracted from the curve of  $(A\hbar\nu)^{1/2}$  plotted as a function of  $\hbar\nu$  (incident photon energy) by extrapolating a tangent line intersected with photon energy axis. Fig. 5(a) shows Tauc plots of the films deposited on sapphire substrate in a working pressure range of 5–40 mTorr. (Note, chemical compositions of these films are the same as the films grown on Si substrate counterpart, which was confirmed by ERDA measurement.) As can be seen in the spectra, the absorption edge shifts apparently towards higher energy when the samples were grown at higher total working pressure, indicating that the bandgap becomes wider as the atomic fraction of O in the film is increased. The extracted bandgap plotted as a function of O atomic fraction is shown in Fig. 5(b). The bandgap increases monotonically (slightly linear) from around 2.22 to 2.66 eV with increasing O atomic fraction from 0.022 to 0.148,

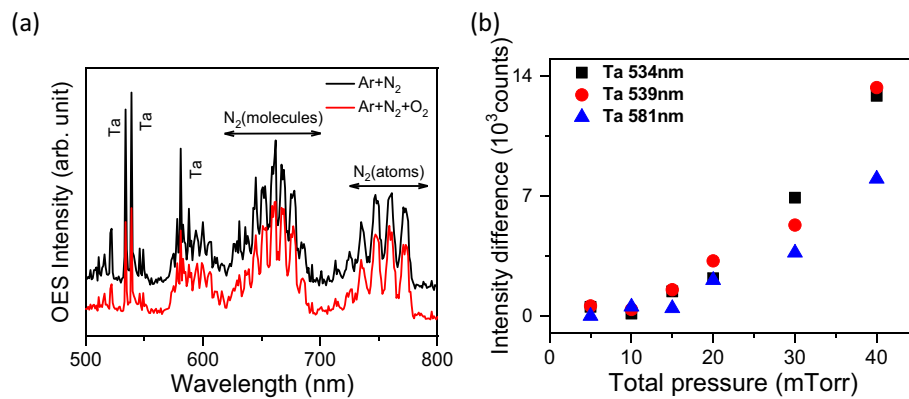


**Fig. 4.** Optical emission spectroscopy (OES) measurement during sputtering. (a) Emission spectra obtained from plasmas generated by sputtered Ta target in two gas mixture, top: Ar + N<sub>2</sub> and bottom: Ar + N<sub>2</sub> + O<sub>2</sub> (O<sub>2</sub>: ~2%), at working pressure ~ 40 mTorr. (b) Pressure dependence of intensity difference of the Ta transition peaks between two gas mixtures.

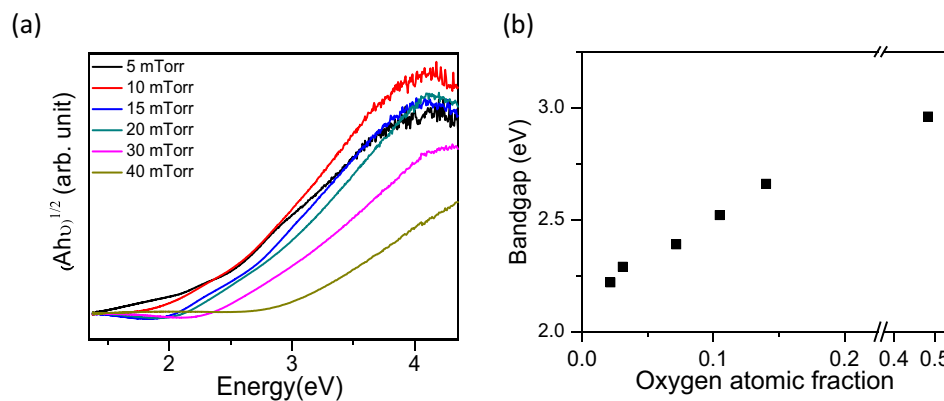


**Fig. 5.** Results of optical absorption spectroscopy (ABS) measurement on the samples grown in pressure range of 5–40 mTorr with a gas mixture of N<sub>2</sub>, Ar, and O<sub>2</sub> (keeping partial pressure of 3:2:0.1). (a) Tauc plot of absorption spectra, and (b) bandgap versus oxygen atomic fraction.

correspondently. The smallest bandgap of the Ta<sub>3-x</sub>N<sub>5-y</sub>O<sub>y</sub> film is very close to the theoretically calculated bandgap of Ta<sub>3</sub>N<sub>5</sub>, 2.0 ± 0.2 eV [4–8]. In addition, a tail at the lower energy side of the absorption edge was also seen in many Ta<sub>3</sub>N<sub>5</sub> films prepared by two-step growth [52]. The band tail, which also called as Urbach energy, is often correlated to the degree of structural disorder and point defects as seen in other semiconductors [53]. When the O atomic fraction raises to 0.483 (40-mTorr sample), the optical bandgap increases to around 2.96 eV. Such a change is reasonable because the crystalline structure and chemical composition of the film have changed to an O-rich TaN<sub>x</sub>O<sub>y</sub> compound, mixed with TaON and Ta<sub>2</sub>O<sub>5</sub>. The absorption is, therefore, more approached to the calculated bandgap of TaON, ~3 eV [7].

According to the calculated electronic density of state (DOS) using DFT methods [7], the valence band of pure Ta<sub>3</sub>N<sub>5</sub> is mainly governed by occupied N 2p states while the conduction band is composed by Ta 5d states. When O atoms substitute for N sites in the structure, the conduction band is still composed by Ta 5d states while the valence band starts to mix O 2p states with occupied N 2p states. Because the O 2p states locate lower in energy than N 2p states, the electronic band gap of Ta<sub>3-x</sub>N<sub>5-y</sub>O<sub>y</sub> becomes broader than pure Ta<sub>3</sub>N<sub>5</sub>. In addition, the substitution of O atoms for N sites is one of the major sources for donating electron and is mainly responsible for the intrinsic n-type conduction [44,52]. At lower-level O incorporation, the donors can form localized states below conduction band minimum. With increasing O atomic fraction, more donated electron can fill the conduction band, which further broadens optical band gap. On the other hand, N vacancies was referred to as another source to form a defect band located slightly deeper below conduction band minimum, giving an absorption band

centered at ~1.72 eV [52]. Although our films always show over stoichiometry with excess N, formation of N vacancies cannot be ruled out. Other defects, such as N, O interstitials and Ta vacancies in the lattice, mostly cause even deep level bands. As to the O-rich TaN<sub>x</sub>O<sub>y</sub> compound, the band gap of monoclinic TaON was predicted to be around 3 eV [7]. DOS calculated by DFT shows that O 2p states become dominant in the valence band. With increasing a bit more N atomic fraction, the bandgap is narrowing towards to 2.5 eV owing to more N 2p states located at higher energy of valence band. Optical properties of TaON films, made by high-power impulse magnetron sputtering, studied by variable angle spectroscopic ellipsometry confirmed that the bandgap increases from 2.5 eV towards to 3.9 eV (Ta<sub>2</sub>O<sub>5</sub>) with increasing O/N ratio [11]. In summary, our OAS result is in consistency with the DFT calculation that substitution of O atoms for N sites in Ta<sub>3-x</sub>N<sub>5-y</sub>O<sub>y</sub> film plays a decisive role on determination of optical properties.

#### 4. Conclusions

Orthorhombic Ta<sub>3-x</sub>N<sub>5-y</sub>O<sub>y</sub> compound films with various atomic fractions grown directly on Si and sapphire substrates using reactive magnetron sputtering on a Ta target was achieved by adjusting total working pressure in a gas mixture of N<sub>2</sub>, Ar, and O<sub>2</sub> (keeping partial pressure of 3:2:0.1). In the pressure regime of 5–30 mTorr, all films were grown in Ta<sub>3</sub>N<sub>5</sub>-type crystal with a low degree of fiber texture along *b*-axis direction. The atomic fraction of O in the films increased from 0.022 to 0.148 as increasing total working pressure, while N decreased with a reverse trend to the O counterpart. The decrement of Ta atomic fraction was counted to be ~0.02 between 5- and 30-mTorr samples. Meanwhile,

*b* lattice constant of the films decreased from 10.30 to 10.17 Å, and optical band gap increased from 2.22 to 2.66 eV with increasing total pressure in the growth. As a result, the O atoms in the films substituted for N sites and the formation of Ta vacancies in the Ta<sub>3</sub>N<sub>5</sub> crystal, resulting in the formation of Ta<sub>3-x</sub>N<sub>5-y</sub>O<sub>y</sub> compounds and the decrement of *b* lattice. For further increasing working pressure to 40 mTorr, the atomic fraction of O increased dramatically to 0.483 in films that comprised mixed amorphous TaON- and Ta<sub>2</sub>O<sub>5</sub>-type compounds, which also leads to the widening of bandgap to ~2.96 eV. The mechanism of increasing O atomic fraction in the film with working pressure is correlated with oxide formed on the Ta target as a result of stronger reactivity of O than N to Ta, and thus reduced the metal sputtering yield, which was evidenced by plasma analysis on sputtering gas. Besides, no pure orthorhombic Ta<sub>3</sub>N<sub>5</sub> phase was formed when the film was grown in a gas mixture of Ar and N<sub>2</sub> without O<sub>2</sub>. Only metallic cubic TaN<sub>x</sub> phases were formed in an over stoichiometric condition with excess N, implying that a small amount of oxygen is required to form Ta<sub>3</sub>N<sub>5</sub>-type structure.

## Funding

This research was funded by Vetenskapsrådet (grant number 2018-04198), Energimyndigheten (grant number 46658-1), and Stiftelsen Olle Engkvist Byggmästare (grant number 197-0210) and the APC was funded by the Linköping University Library. The Swedish Government Strategic Research Area in Materials Science on Functional Materials at Linköping University (Faculty Grant SFO-Mat-LiU 2009-00971) is acknowledged for financial support. Support by VR-RFI (contracts #821-2012-5144 & #2017-00646\_9) and the Swedish Foundation for Strategic Research (SSF, contract RIF14-0053 and SE13-0333) for accelerator operation at Uppsala University is gratefully acknowledged.

## CRediT authorship contribution statement

Conceptualization, J.-C.C., J.B., and C.-L.H.; methodology, J.-C.C., F.E., M.A.S., G.G., Z.H. and C.-L.H.; resources, D.P. J.B., L.H., and C.-L.H.; data curation J.-C.C., F.E., M.A.S., G.G., and Z.H.; writing—original draft preparation, J.-C.C. and C.-L.H.; writing—review and editing, J.-C.C., F.E., M.A.S., G.G., Z.H., D.P. J.B., L.H., and C.-L.H.; project administration, C.-L.H.; funding acquisition, C.-L.H., L.H., and J.B. All authors have contributed to the writing and agreed to the published version of the manuscript.

## Declaration of competing interest

The authors declare that they have no known competing financial interests or personal relationships that could have appeared to influence the work reported in this paper.

## References

- [1] A. Fujishima, K. Honda, Electrochemical photolysis of water at a semiconductor electrode, *Nature* 238 (1972) 37–38.
- [2] Y. Yang, S. Niu, D. Han, T. Liu, G. Wang, Y. Li, Progress in developing metal oxide nanomaterials for photoelectrochemical water splitting, *Adv. Energy Mater.* 7 (2017), 1700555.
- [3] V.M. Aroutiounian, V.M. Arakelyan, G.E. Shahnazaryan, Metal oxide photoelectrodes for hydrogen generation using solar radiation-driven water splitting, *Sol. Energy* 78 (2005) 581–592.
- [4] M. Hara, E. Chiba, A. Ishikawa, T. Takata, J.N. Kondo, K. Domen, Ta<sub>3</sub>N<sub>5</sub> and TaON thin films on Ta foil: surface composition and stability, *J. Phys. Chem. B* 107 (2003) 13441–13445.
- [5] M. Hara, G. Hitoki, T. Takata, J.N. Kondo, H. Kobayashi, K. Domen, TaON and Ta<sub>3</sub>N<sub>5</sub> as new visible light driven photocatalysts, *Catal. Today* 78 (2003) 555–560.
- [6] W.-J. Chun, A. Ishikawa, H. Fujisawa, T. Takata, J.N. Kondo, M. Hara, M. Kawai, Y. Matsumoto, K. Domen, Conduction and valence band positions of Ta<sub>2</sub>O<sub>5</sub>, TaON, and Ta<sub>3</sub>N<sub>5</sub> by UPS and electrochemical methods, *J. Phys. Chem. B* 107 (2003) 1798–1803.
- [7] M. Harb, P. Sautet, E. Nurlaela, P. Raybaud, L. Cavallo, K. Domen, J.-M. Basset, K. Takane, Tuning the properties of visible-light-responsive tantalum (oxy) nitride photocatalysts by nonstoichiometric compositions: a first-principles viewpoint, *Phys. Chem. Chem. Phys.* 16 (2014), 20548.
- [8] M. Rudolph, D. Stanesco, J. Alvarez, E. Foy, J.-P. Kleider, H. Magnan, T. Minea, N. Herlin-Boime, B. Bouchet-Fabre, M.-C. Hugon, The role of oxygen in magnetron-sputtered Ta<sub>3</sub>N<sub>5</sub> thin films for the photo electrolysis of water, *Surf. Coat. Technol.* 324 (2017) 620–625.
- [9] J.M. Morbec, I. Narkeviciute, T.F. Jaramillo, G. Galli, Optoelectronic properties of Ta<sub>3</sub>N<sub>5</sub>: a joint theoretical and experimental study, *Phys. Rev. B* 90 (2014), 155204.
- [10] A.B. Murphy, P.R.F. Barnes, L.K. Randeniya, I.C. Plumb, I.E. Grey, M.D. Horne, A. Glasscock, Efficiency of solar water splitting using semiconductor electrodes, *Int. J. Hydrog. Energy* 31 (2006) 1999–2017.
- [11] J. Čapek, S. Batková, S. Haviar, J. Houška, R. Čerstvý, P. Zeman, Effect of annealing on structure and properties of Ta–O–N films prepared by high power impulse magnetron sputtering, *Ceram. Int.* 45 (2019) 9454–9461.
- [12] J. Čapek, S. Batková, M. Matas, S. Kos, T. Kozák, S. Haviar, J. Houška, J. Schusser, J. Minář, F. Dvořák, P. Zeman, Bixbyite-Ta<sub>3</sub>N<sub>2</sub>O film prepared by HiPIMS and postdeposition annealing: structure and properties, *J. Vac. Sci. Technol. A* 38 (2020) 033409.
- [13] A. Dabirian, R. van de Krol, Resonant optical absorption and defect control in Ta<sub>3</sub>N<sub>5</sub> photoanodes, *Appl. Phys. Lett.* 102 (2013), 033905.
- [14] H. Hajibabaei, D.J. Little, A. Pandey, D. Wang, Z. Mi, T.W. Hamann, Direct deposition of crystalline Ta<sub>3</sub>N<sub>5</sub> thin films on FTO for PEC water splitting, *ACS Appl. Mater. Interfaces* 11 (2019) 15457–15466.
- [15] I. Narkeviciute, P. Chakthranont, A.J.M. Mackus, C. Hahn, B.A. Pinaud, S.F. Bent, T.F. Jaramillo, Tandem core–shell Si–Ta<sub>3</sub>N<sub>5</sub> photoanodes for photoelectrochemical water splitting, *Nano Lett.* 16 (2016) 7565–7572.
- [16] M. Rudolph, A. Demeter, E. Foy, V. Tiron, L. Sirghi, T. Minea, B. Bouchet-Fabre, M.-C. Hugon, Improving the degree of crystallinity of magnetron-sputtered Ta<sub>3</sub>N<sub>5</sub> thin films by augmenting the ion flux onto the substrate, *Thin Solid Films* 636 (2017) 48–53.
- [17] A. Ishihara, S. Doi, S. Mitsushima, K.-i. Ota, Tantalum (oxy)nitrides prepared using reactive sputtering for new nonplatinum cathodes of polymer electrolyte fuel cell, *Electrochim. Acta* 53 (2008) 5442–5450.
- [18] D. Yokoyama, H. Hashiguchi, K. Maeda, T. Minegishi, T. Takata, R. Abe, J. Kubota, K. Domen, Ta<sub>3</sub>N<sub>5</sub> photoanodes for water splitting prepared by sputtering, *Thin Solid Films* 519 (2011) 2087–2092.
- [19] N. Izyumskaya, V. Avrutin, K. Ding, Ü. Özgür, H. Morkoç, H. Fujioka, Emergence of high quality sputtered III-nitride semiconductors and devices, *Semicond. Sci. Technol.* 34 (2019), 093003.
- [20] E.A. Serban, J. Palisaitis, M. Junaid, L. Tengdelius, H. Högberg, L. Hultman, P.O. Å. Persson, J. Birch, C.L. Hsiao, Magnetron sputter epitaxy of high-quality GaN nanorods on functional and cost-effective templates/substrates, *Energies* 10 (2017) 1322.
- [21] M. Junaid, C.L. Hsiao, J. Palisaitis, J. Jensen, P.O. Å. Persson, L. Hultman, J. Birch, Electronic-grade GaN(0001)/Al<sub>2</sub>O<sub>3</sub>(0001) grown by reactive DC-magnetron sputter epitaxy using a liquid Ga target, *Appl. Phys. Lett.* 98 (2011) 7–10.
- [22] C.M. Koller, H. Marihart, H. Bolvardi, S. Kolozsvári, P.H. Mayrhofer, Structure, phase evolution, and mechanical properties of DC, pulsed DC, and high power impulse magnetron sputtered Ta–N films, *Surf. Coat. Technol.* 347 (2018) 304–312.
- [23] N. Terao, Structure of tantalum nitrides, *Jpn. J. Appl. Phys.* 10 (1971) 248.
- [24] J. Etourneau, J. Portier, F. Ménil, The role of the inductive effect in solid state chemistry: how the chemist can use it to modify both the structural and the physical properties of the materials, *J. Alloys Compd.* 188 (1992) 1–7.
- [25] E.A. Serban, P.O. Å. Persson, I. Poenaru, M. Junaid, L. Hultman, J. Birch, C.L. Hsiao, Structural and compositional evolutions of In<sub>x</sub>Al<sub>1-x</sub>N core–shell nanorods grown on Si (111) substrates by reactive magnetron sputter epitaxy, *Nanotechnology* 26 (2015) 215602.
- [26] A. Pradaswara, J. Birch, M. Junaid, E.A. Serban, L. Hultman, C.-L. Hsiao, Review of GaN thin film and nanorod growth using magnetron sputter epitaxy, *Appl. Sci.* 10 (2020) 3050.
- [27] P.J. Kelly, R.D. Arnell, Magnetron sputtering: a review of recent developments and applications, *Vacuum* 56 (2000) 159–172.
- [28] C.L. Hsiao, J. Palisaitis, M. Junaid, R.-S. Chen, P.O. Å. Persson, P. Sandström, P.-O. Holtz, L. Hultman, J. Birch, Spontaneous formation of AlInN coreshell nanorod arrays by ultrahigh-vacuum magnetron sputter epitaxy, *Appl. Phys. Exp.* 4 (2011), 115002.
- [29] G. Greczynski, D. Primetzhofer, J. Lu, L. Hultman, Core-level spectra and binding energies of transition metal nitrides by non-destructive X-ray photoelectron spectroscopy through capping layers, *Appl. Surf. Sci.* 396 (2017) 347–358.
- [30] G. Greczynski, L. Hultman, X-ray photoelectron spectroscopy: towards reliable binding energy referencing, *Prog. Mater. Sci.* 107 (2020), 100591.
- [31] G. Greczynski, L. Hultman, Compromising science by ignorant instrument calibration—need to revisit half a century of published XPS data, *Angew. Chem. Int. Ed.* 59 (2020) 5002.
- [32] M. to Baben, M. Hans, D. Primetzhofer, S. Evertz, H. Ruess, J.M. Schneider, Unprecedented thermal stability of inherently metastable titanium aluminum nitride by point defect engineering, *Mater. Res. Lett.* 5 (2017) 158–169.
- [33] Q.Y. Zhang, X.X. Mei, D.Z. Yang, F.X. Chen, T.C. Ma, Y.M. Wang, F.N. Teng, Preparation, structure and properties of TaN and TaC films obtained by ion beam assisted deposition, *Nucl. Instr. Meth. Phys. Res. B* 127–128 (1997) 664–668.
- [34] R. Li, Y. Qin, G. Liu, C. Zhang, H. Liang, Y. Qing, Y. Zhang, K. Zhang, Tantalum nitride coatings prepared by magnetron sputtering to improve the bioactivity and osteogenic activity for titanium alloy implants, *RSC Adv.* 7 (2017) 55408.
- [35] N. Arshi, J. Lu, Y.K. Joo, J.H. Yoon, B.H. Koo, Effects of nitrogen composition on the resistivity of reactively sputtered TaN thin films, *Surf. Interface Anal.* 47 (2015) 154–160.



- [36] M. Alishahi, F. Mahboubi, S.M. Mousavi Khoie, M. Aparicio, E. Lopez-Elvira, J. Méndez, R. Gago, Structural properties and corrosion resistance of tantalum nitride coatings produced by reactive DC magnetron sputtering, *RSC Adv.* 6 (2016) 89061–89072.
- [37] Y. Cong, H.S. Park, S. Wang, H.X. Dang, F.-R.F. Fan, C.B. Mullins, A.J. Bard, Synthesis of Ta<sub>3</sub>N<sub>5</sub> nanotube arrays modified with electrocatalysts for photoelectrochemical water oxidation, *J. Phys. Chem. C* 116 (2012) 14541–14550.
- [38] S. Khan, M.J.M. Zapata, M.B. Pereira, R.V. Gonçalves, L. Strizik, J. Dupont, M.J. L. Santos, S.R. Teixeira, Structural, optical and photoelectrochemical characterizations of monoclinic Ta<sub>3</sub>N<sub>5</sub> thin films, *Phys. Chem. Chem. Phys.* 17 (2015), 23952.
- [39] S. Khan, S.R. Teixeira, M.J.L. Santos, Controlled thermal nitridation resulting in improved structural and photoelectrochemical properties from Ta<sub>3</sub>N<sub>5</sub> nanotubular photoanodes, *RSC Adv.* 5 (2015), 103284.
- [40] D. Cristea, L. Cunha, C. Gabor, I. Ghiuta, C. Croitoru, A. Marin, L. Velicu, A. Besleaga, B. Vasile, Tantalum oxynitride thin films: assessment of the photocatalytic efficiency and antimicrobial capacity, *Nanomaterials* 9 (2019) 476.
- [41] D. Li, F. Tian, D. Duan, K. Bao, B. Chu, X. Sha, B. Liu, T. Cui, Mechanical and metallic properties of tantalum nitrides from first-principles calculations, *RSC Adv.* 4 (2014) 10133.
- [42] O. Kerrec, D. Devilliers, H. Groult, P. Marcus, Study of dry and electrogenerated Ta<sub>2</sub>O<sub>5</sub> and Ta/Ta<sub>2</sub>O<sub>5</sub>/Pt structures by XPS, *Mater. Sci. Eng. B* 55 (1998) 134.
- [43] S.J. Henderson, A.L. Hector, Structural and compositional variations in Ta<sub>3</sub>N<sub>5</sub> produced by high-temperature ammonolysis of tantalum oxide, *J. Solid State Chem.* 179 (2006) 3518–3524.
- [44] T. Jing, Y. Dai, X. Ma, W. Wei, B. Huang, Effects of intrinsic defects and extrinsic doping on the electronic and photocatalytic properties of Ta<sub>3</sub>N<sub>5</sub>, *RSC Adv.* 5 (2015) 59390.
- [45] C.L. Hsiao, J. Palisaitis, M. Junaid, P.O.Å. Persson, J. Jensen, Q.X. Zhao, L.C. Chen, K.H. Chen, J. Birch, Room-temperature heteroepitaxy of single-phase Al<sub>1-x</sub>In<sub>x</sub>N films with full composition range on isostructural wurtzite substrates, *Thin Solid Films* 524 (2012) 113.
- [46] R.D. Shannon, Revised effective ionic radii and systematic studies of interatomic distances in halides and Chalcogenides, *Acta Cryst. A* 32 (1976) 751.
- [47] W.F. Meggers, C.H. Corliss, B.F. Scribner, Tables of spectral-line intensities, part I – arranged by elements, *Natl. Bur. Stand. Monograph* 145, Nat. Bur. Stand., U.S. (1975) 246.
- [48] D. Popović, V. Milosavljević, S. Daniels, Practical sensor for nitrogen in direct current glow discharges, *J. Appl. Phys.* 102 (2007), 103303.
- [49] G.L. Humphrey, Heats of formation of tantalum, niobium and zirconium oxides, and tantalum carbide, *J. Am. Chem. Soc.* 76 (1953) 978–980.
- [50] A.D. Mah, N.L. Gellert, Heats of formation of niobium nitride, tantalum nitride and zirconium nitride from combustion calorimetry, *J. Am. Chem. Soc.* 78 (1956) 3261–3263.
- [51] J.B. Coulter, D.P. Birnie III, Assessing Tauc plot slope quantification: ZnO thin films as a model system, *Phys. Status Solidi B* 255 (2018), 1700393.
- [52] J. Wang, A. Ma, Z. Li, J. Jiang, J. Feng, Z. Zou, Effects of oxygen impurities and nitrogen vacancies on the surface properties of the Ta<sub>3</sub>N<sub>5</sub> photocatalyst: a DFT study, *Phys. Chem. Chem. Phys.* 17 (2015) 23265.
- [53] A.S. Hassanien, A.A. Akl, Influence of composition on optical and dispersion parameters of thermally evaporated non-crystalline Cd<sub>50</sub>S<sub>50-x</sub>Se<sub>x</sub> thin films, *J. Alloys Compd.* 648 (2015) 280–290.